Proxy-Based Optimal Control Allocation for Dual-Input Over-Actuated Systems

Molong Duan, *Student Member, IEEE*, and Chinedum E. Okwudire, *Member, IEEE*

***Abstract*—Over-actuated systems are characterized by a larger number of actuators compared with the degrees of freedom to be controlled. In such systems, it is often desirable to allocate control effort dynamically (i.e., over a broad range of frequencies) in an optimal manner, without sacrificing control performance. At present, this goal is achieved through computationally intensive real-time optimization or by using static redundancy models, which could significantly sacrifice optimality and/or control performance. In the context of dual-input, single-output over-actuated systems, this paper proposes a proxy-based approach for optimal dynamic control allocation without need for real-time optimization. Using factorization, a causally implementable optimal relationship between two control inputs is derived. It is shown that control energy is minimized indirectly by minimizing the deviation of control inputs from the derived relationship, which can be achieved using classical or advanced feedforward (FF) and/or feedback (FB) control techniques. A classical FF and FB approach for implementing the proposed proxy-based allocation scheme, alongside an approach for handling input constraints, is detailed and validated in simulations and experiments on an over-actuated hybrid feed drive. In comparison with an existing static-model-based dynamic allocation approach, large reductions in control energy without sacrificing control performance are demonstrated.**

***Index Terms*—Dynamic control allocation, energy optimality, over-actuated system, proxy-based control.**

I. Introduction

OVER-ACTUATED systems are characterized by a larger number of actuators compared with the degrees of freedom (DOFs) to be controlled [1]. They are widely used in aerospace, manufacturing, robotics and other control applications to enhance fault tolerance, energy efficiency, accuracy, etc. [2]–[9]. For example, redundant thrusters are employed in spacecraft to ensure maneuverability in the event of thruster failure [4]. In servo systems, over-actuation is used to improve motion range [2], accuracy [7] and/or efficiency [8]. Over-actuation also provides a promising solution to structural flexibility issues in lightweight motion systems envisioned for the manufacture of next-generation integrated circuits [3].

A major focus in controlling over-actuated systems is control (effort) allocation, i.e., how to best utilize redundant control inputs to achieve desired outputs [10]. This is often achieved using a two-stage framework, having a high-level nominal controller (a.k.a. "virtual controller" [5], [10]–[12]), which determines the overall control effort required to achieve the desired output trajectories, and a control allocator designed to best distribute the control effort to the actuators [10]–[14]. The criterion for determining the best distribution in over-actuated systems could vary from problem to problem but a very common criterion, widely adopted in the literature, is to minimize the 2-norm (i.e., control energy) of the control inputs [5], [6], [10]–[16]. References to control allocation in the rest of this paper specifically pertain to this common practice of energy optimal control allocation.

Several works have focused on control allocation for systems with strong input redundancy, where there exists a set of control inputs that do not affect system internal states [11]–[14]. In strongly input redundant systems, control allocation boils down to a quadratic programming problem with linear constraints, which can be solved using several numerical techniques [14]. Strong redundancy is however a very restrictive condition, which, in practice, often requires exact collocation of actuators or severe truncation of higher order dynamics [12]. A more general and tenable form of redundancy is weak input redundancy, where there exist a set of control inputs which do not alter system outputs, though they may alter system internal states [15]–[17]. Control allocation is more challenging for weakly redundant systems because the constraints posed by allocation are dynamic rather than static (as is the case for strongly redundant systems). A general approach for addressing control allocation for weakly redundant systems is to use a model predictive control framework [16]; however, this often leads to computationally expensive real-time optimization. Using regulator theory, Galeani *et al*. [17] explored static state feedback (FB) structures for optimal control allocation in weakly input redundant systems, by minimizing the infinity norm of the control efforts; a finite dimension relaxation was employed to reduce the computational cost. However, this relaxation leads to a hybrid system, and the associated switching events may introduce undesirable transients. Zaccarian [15] proposed a dynamic allocation method based on a static redundancy model in weakly input redundant systems. While this approach [15] greatly simplifies the problem and reduces computational

Manuscript received January 9, 2017; revised May 26, 2017, September 4, 2017, and October 24, 2017; accepted January 2, 2018. Date of publication January 23, 2018; date of current version April 16, 2018. Recommended by Technical Editor L. Wu. This work was supported by the National Science Foundation, Dynamically Adaptive Feed Drives for Smart and Sustainable Manufacturing, under CAREER Award 1350202. *(Corresponding author: Chinedum E. Okwudire.)*

The authors are with the University of Michigan, Ann Arbor, MI 48109 USA (e-mail: molong@umich.edu; okwudire@umich.edu).

Color versions of one or more of the figures in this paper are available online at http://ieeexplore.ieee.org.

Digital Object Identifier 10.1109/TMECH.2018.2796500

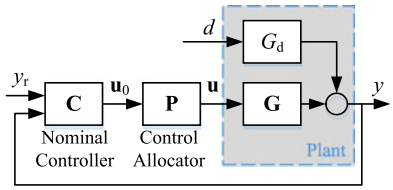

Fig. 1. Generalized block diagram for control allocation for dual-input, single-output plant.

burden, it is incapable of optimal broadband control allocation. Moreover, given an accurate plant model, the approaches in [15] and [17] both cannot guarantee invariance of the controlled output (i.e., control performance) during broadband control allocation due to their statically defined null space. In the context of dual-input, single-output systems, the present authors derived an optimal transfer function relationship between two control inputs [18], [19]. They showed that energy optimal allocation can be achieved for weakly input redundant systems, without sacrificing control performance, by constraining the ratio of control inputs to satisfy the derived relationship. However, the derived relationship is in general noncausally implementable [19]. To address this challenge, they propose a causal stable approximation of the relationship, which is used in a preliminary allocator design in [20]. The loss of optimality due to this approximation is quantitatively studied in [19].

Building on these preliminary works, the contributions of this paper are as follows.

1) A causally implementable control proxy is proposed and is shown to be an accurate measure of deviation from energy optimality, i.e., it has no approximation errors.
2) It is shown that optimal broadband control allocation can be achieved, without need for real-time optimization, by using standard feedforward (FF) and FB techniques to regulate the proxy.
3) An actuator constraint handling method is proposed within the proposed allocation framework.

The rest of the paper is organized as follows. A formal problem statement is provided in Section II. In Section III, the proxy is introduced and mathematically analyzed. Based on the analysis, a proxy-based control allocation scheme with constraint handling is proposed, along with classical feedforward (FF) and FB implementations of the allocation scheme. In Section IV, the proposed allocator is validated in simulations and experiments on an over-actuated hybrid feed drive system. Conclusions and future work are presented in Section V.

II. Problem Statement

Assume a dual-input, single-output LTI plant shown in Fig. 1, given by

$$y = \mathbf{G}\mathbf{u} + G_{\mathrm{d}} d \tag{1}$$

where $\mathbf{G} = [G_1,\ G_2]$; y, $\mathbf{u} = [u_1,\ u_2]^T$, and d are respectively the system output, control inputs and disturbance input; both u_1 and u_2 are assumed to belong to L^2 space and has zero initial values. According to [15], [17], such a system with more inputs than outputs is defined as weakly input redundant if changes in its inputs do not necessarily change its output, i.e.

$$\mathrm{Ker}\left(\mathbf{G}\left(s\right)\right) \neq \varnothing \tag{2}$$

where s is the Laplace variable and Ker indicates the kernel (null space) of the associated matrix. Note that in (2), and in the rest of this paper, weak redundancy is defined in its dynamic (broadband) sense rather than its static sense (as $s \rightarrow 0$) as in [15]. In weakly input redundant systems, there exists a family of input trajectories that yield the same output trajectory due to redundancy [15], [16]. Assuming a nominal control input $\mathbf{u}_0$ (e.g., from a virtual controller [10]) yields a desirable output y_0 under disturbance d_0, i.e.

$$\mathbf{G}\mathbf{u}_0 = y_0 - G_{\mathrm{d}} d_0. \tag{3}$$

The family of control signals that replicate y_0 under d_0 defines a set Ω, given by

$$\Omega\left(\mathbf{u}_0\right) \triangleq \left\{\mathbf{u} \in \mathbb{R}^2 : \mathbf{G}\left(\mathbf{u}_0 - \mathbf{u}\right) = 0\right\}. \tag{4}$$

Set Ω is the nonempty control input space for optimization of the over-actuated system and can be calculated by establishing the orthogonal complement of system $\mathbf{G}$. As shown in Fig. 1, the goal of energy optimal control allocation is to formulate a mapping $\mathbf{P}$ between $\mathbf{u}_0$ and $\mathbf{u} \in \Omega$ such that control energy is minimized, under the influence of disturbance d_0, without altering $y = y_0$. Note that the influence of reference signal y_{r}, in Fig. 1, is embedded in $\mathbf{u}_0$; hence, y_{r} is not explicitly considered in the problem formulation.

Assume the typical quadratic control energy cost functional

$$J \triangleq \int \left(\mathbf{u}^T \mathbf{R}\mathbf{u}\right) dt = \int \begin{bmatrix} u_1 \\ u_2 \end{bmatrix}^T \begin{bmatrix} R_{11} & R_{12} \\ R_{12} & R_{22} \end{bmatrix} \begin{bmatrix} u_1 \\ u_2 \end{bmatrix} dt \tag{5}$$

where $\mathbf{R}$ is a positive definite square symmetric matrix which, in general, is a design parameter. However, in certain scenarios, $\mathbf{R}$ can be determined by physical properties of the actuators. To achieve optimality, the variation of J should satisfy

$$\delta J = 0 \Rightarrow \int \left(\delta\mathbf{u}^T \mathbf{R}\mathbf{u}\right) dt = 0 \tag{6}$$

where $\delta\mathbf{u} = [\delta u_1,\ \delta u_2]^T$. Moreover, based on (4), the variation of every member of set Ω should satisfy the relationship

$$G_1 \delta u_1 + G_2 \delta u_2 = 0. \tag{7}$$

Combining (6) and (7), we get

$$\begin{aligned} &\int \left(R_{11} u_1 \delta u_1 + R_{12}(-u_1 (G_2{}^{-1} G_1 \delta u_1) + u_2 \delta u_1)\right. \\ &\quad \left. - R_{22} u_2 G_2{}^{-1} G_1 \delta u_1\right) dt = 0 \\ &\Rightarrow \int \left(R_{11} u_1 + R_{12}(-(G_2{}^{-1} G_1)^* u_1 + u_2)\right. \\ &\quad \left. - R_{22}(G_2{}^{-1} G_1)^* u_2\right) \delta u_1 dt = 0 \end{aligned} \tag{8}$$

where superscript * represents the adjoint operator; the frequency response of the adjoint system is the complex conjugate of the original system at every frequency [21]. According to the fundamental lemma of calculus of variations [22], the integrand

of (8) must be equal to zero at all time, which yields the energy optimal control (input) ratio

$$\beta^*(s) \triangleq \frac{\hat{u}_1(s)}{\hat{u}_2(s)} = \frac{R_{22}G_1^* - R_{12}G_2^*}{R_{11}G_2^* - R_{12}G_1^*} \tag{9}$$

where the ˆ accent is used to denote optimality. Note that (9) is a more general form of the optimal ratio derived in [18] and [19], which is shown in [19] to be, in general, noncausally implementable. A causal stable approximation of β^* (denoted as β) was proposed by the authors in prior work [18], [19] as a solution to this problem. However, this approximation is only valid where the frequency response of β satisfies one of following conditions: $|\beta(j\omega)| >> 1$, $|\beta(j\omega)| << 1$ or $\angle\beta(j\omega) \approx n\pi$ $(n \in \mathbb{Z})$ [19]. Significant deviations from energy optimality could result if these conditions are not met, and there is no guarantee that energy optimality is always improved as u_1/u_2 approaches β. Moreover, the approach presented in [18] and [19] was predicated on H_2/H_∞ optimal control and full state FB, which may not always be feasible nor desirable. Building on preliminary work reported in [20], the rest of this paper presents an approach that overcomes the highlighted challenges of the authors' prior work. A more general and elegant strategy for optimal dynamic control allocation for control energy is proposed; it could be implemented using advanced controllers like H_2/H_∞ [18], or with low computational burden and complexity using classical FF and/or FB controllers.

III. Proposed Proxy-Based, Energy Optimal Dynamic Allocation Approach

A. Causal Alignment Deviation from Optimal Control Ratio

Given the optimal control ratio (β^*) defined in the preceding section, we seek an allocator $\mathbf{P}$ that enforces the condition $u_1 - \beta^* u_2 = 0$. The operator s has adjoint $s^* = -s$ [21], since the signals it operates on (i.e., u_1 and u_2) belong to the L^2 space and has zero initial and final values. This assumption is valid for control signal $\mathbf{u}$ in almost all practical situations; hence, it is adopted here. Accordingly, a causal implementation of $\beta^*(s)$ involves the evaluation of $\beta(-s)$ [23], which contains unstable poles. We address this challenge by defining u_D, a causal stable measure of the deviation of u_1/u_2 from β^*, as

$$u_\mathrm{D} = \beta_2 u_1 - \beta_1 u_2 \tag{10}$$

where β_1 and β_2 represent a factorization of β^* defined as

$$\beta^* = \frac{\beta_1}{\beta_2} = \left(\underbrace{\frac{R_{22}G_{1\mathrm{n}}^* - R_{12}G_{2\mathrm{n}}^*}{\psi}}_{\triangleq\beta_1}\right)\left(\underbrace{\frac{R_{11}G_{2\mathrm{n}}^* - R_{12}G_{1\mathrm{n}}^*}{\psi}}_{\triangleq\beta_2}\right)^{-1}. \tag{11}$$

Here $G_{1\mathrm{n}}$ and $G_{2\mathrm{n}}$ are, respectively, the coprime numerators of G_1 and G_2 (i.e., $\mathbf{G} = [G_{1\mathrm{n}},\ G_{2\mathrm{n}}]/D_\mathrm{ol}$, where D_ol is defined such that $G_{1\mathrm{n}}$ and $G_{2\mathrm{n}}$ do not have shared zeros). On the other hand, ψ is a causal stable denominator, whose selection is discussed in the following section.

The implication of the proposed decomposition of β^* is that its noncausally implementable denominator is replaced by the causal stable denominator, ψ, of β_1 and β_2. Note that $G_{1\mathrm{n}}^*(s) = G_{1\mathrm{n}}(-s)$ and $G_{2\mathrm{n}}^*(s) = G_{2\mathrm{n}}(-s)$ can induce nonminimum phase (NMP) zeros in β_1 and β_2, but they do not make β_1 and β_2 unstable. Therefore, β_1 and β_2, unlike β^*, are causally implementable; hence the alignment deviation, u_D, is determinable by a control system in real time.

B. Relationship Between Alignment Deviation and Control Energy Optimality

Based on (10), the alignment deviation, u_D, can be viewed as a proxy signal which is usable by a control allocator to indirectly achieve control energy optimality. It is therefore instrumental to understand the relationship between u_D and J. To do this, for any control input $\mathbf{u} = (\hat{\mathbf{u}} + \delta\mathbf{u}) \in \Omega(\hat{\mathbf{u}})$, J can be decomposed as follows:

$$J(\mathbf{u}) = \underbrace{\int \hat{\mathbf{u}}^T\mathbf{R}\hat{\mathbf{u}}dt}_{\hat{J}} + \underbrace{2\int \delta\mathbf{u}^T\mathbf{R}\hat{\mathbf{u}}dt}_{J_\mathrm{cc}} + \underbrace{\int \delta\mathbf{u}^T\mathbf{R}\delta\mathbf{u}dt}_{\Delta J} \tag{12}$$

where $\hat{J}$ and ΔJ are positive definite terms representing the optimal value of J and the energy of deviation $\delta\mathbf{u}$ (i.e., $J(\delta\mathbf{u})$), respectively, while J_cc is a cross-coupling term between $\delta\mathbf{u}$ and $\hat{\mathbf{u}}$. Based on (9), the energy optimal control, $\hat{\mathbf{u}}$, can be written as

$$\hat{\mathbf{u}} = \begin{bmatrix}\hat{u}_1\\ \hat{u}_2\end{bmatrix} = \begin{bmatrix}R_{22}G_1^* - R_{12}G_2^*\\ R_{11}G_2^* - R_{12}G_1^*\end{bmatrix} e_0 \tag{13}$$

where e_0 is a basis signal. Applying (7) and (13) to J_cc, we get

$$\begin{aligned} J_\mathrm{cc} &= 2\int \delta\mathbf{u}^T\mathbf{R}\hat{\mathbf{u}}dt \\ &= 2\left(R_{11}R_{22} - {R_{12}}^2\right)\int \left(\delta u_1\left({G_1}^* e_0\right) + \delta u_2\left({G_2}^* e_0\right)\right)dt \\ &= 2\left(R_{11}R_{22} - {R_{12}}^2\right)\int \underbrace{\left(G_1\delta u_1 + G_2\delta u_2\right)}_{\equiv 0} e_0 dt = 0 \end{aligned} \tag{14}$$

meaning that $J = \hat{J} + \Delta J$. Knowing that $u_\mathrm{D} = 0$ when $\mathbf{u} = \hat{\mathbf{u}}$, (10) can be rewritten as

$$u_\mathrm{D} = \beta_2\delta u_1 - \beta_1\delta u_2. \tag{15}$$

Extracting the numerator of (7) and combining it with (15), u_D can also be written in terms of δu_1 and δu_2 as

$$\begin{cases}\left(\beta_1 G_{1\mathrm{n}} + \beta_2 G_{2\mathrm{n}}\right)\delta u_1 = G_{2\mathrm{n}} u_\mathrm{D}\\ \left(\beta_1 G_{1\mathrm{n}} + \beta_2 G_{2\mathrm{n}}\right)\delta u_2 = -G_{1\mathrm{n}} u_\mathrm{D}\end{cases}. \tag{16}$$

Based on β_1 and β_2 defined in (11), the following relationship is derived:

$$\beta_1 G_{1\mathrm{n}} + \beta_2 G_{2\mathrm{n}} = \frac{\Pi}{\psi} \tag{17}$$

where

$$\Pi \triangleq \begin{bmatrix}G_{2\mathrm{n}}^*\\ -G_{1\mathrm{n}}^*\end{bmatrix}^T \mathbf{R} \begin{bmatrix}G_{2\mathrm{n}}\\ -G_{1\mathrm{n}}\end{bmatrix}. \tag{18}$$

Applying Parseval's theorem and the frequency-domain expression of (15) to (17), the energy increment ΔJ can be expressed as

$$\Delta J = \int \delta \mathbf{u}^T \mathbf{R} \delta \mathbf{u} dt = \frac{1}{2\pi} \int \delta \mathbf{u}^* (\omega) \mathbf{R} \delta \mathbf{u} (\omega) d\omega$$
$$= \frac{1}{2\pi} \int \frac{\psi^* \psi}{\Pi} u_{\mathrm{D}}^* u_{\mathrm{D}} d\omega. \tag{19}$$

This leads to the relationship

$$\Delta J = \|u_{\mathrm{D}}\|_2^2 \tag{20}$$

if ψ is selected such that $\psi^* \psi = \Pi$. The implication of (20) is that the deviation of u_{D} from zero, measured by $\|u_{\mathrm{D}}\|_2^2$, equals the deviation of J from its optimal value of $\hat{J}$. While the selection $\psi^* \psi = \Pi$ may be mathematically convenient, a question that remains is whether it is a causal stable choice for ψ. Notice from (18) that Π is self-adjoint (i.e., $\Pi^* = \Pi$); it consists only of zeros, with each zero having a mirror image on the opposite side of the imaginary axis of the s plane. One can therefore collect all the minimum phase zeros of Π into ψ, leading to a stable and causally implementable ψ. Note that $\mathbf{R}$ is positive definite, indicating based on (18) that

$$\Pi (j\omega) = \begin{bmatrix} G_{2\mathrm{n}} (-j\omega) \\ -G_{1\mathrm{n}} (-j\omega) \end{bmatrix}^T \mathbf{R} \begin{bmatrix} G_{2\mathrm{n}} (j\omega) \\ -G_{1\mathrm{n}} (j\omega) \end{bmatrix} < 0 \tag{21}$$

holds for all $s = j\omega$. Therefore, Π has no zeros on the imaginary axis ($\Pi(j\omega) \neq 0$) as long as $G_{1\mathrm{n}}$ and $G_{2\mathrm{n}}$ do not share common zeros on the imaginary axis, which is satisfied due to the fact that $G_{1\mathrm{n}}$ and $G_{2\mathrm{n}}$ are coprime.

C. General Structure of Proposed Control Allocation Scheme and Representative Implementations

Referring to Fig. 1, control allocator $\mathbf{P}$ is any mapping between $\mathbf{u}_0$ and $\mathbf{u} \in \Omega(\mathbf{u}_0)$. Based on (4), $\mathbf{u}_0 - \mathbf{u}$ belongs to the orthogonal complement of $\mathbf{G}$ and thus $\mathbf{u}$ is explicitly written as

$$\mathbf{G} (\mathbf{u}_0 - \mathbf{u}) = 0 \Rightarrow \mathbf{u} = \mathbf{u}_0 + \begin{bmatrix} -G_2 \\ G_1 \end{bmatrix} H_v v \tag{22}$$

where v is an arbitrary signal while H_v is a user-defined prefilter that can be applied to v (e.g., to attenuate high-frequency model mismatch). Following the discussions in Section III-A and B, the desire to make $\mathbf{P}$ an energy-optimal dynamic allocator can be indirectly achieved through regulation of u_{D}. This can be achieved through FF and/or FB control, shown in Fig. 2 as H_{ff} and H_{fb}, respectively. Note that the Sat$(\cdot)$ block and dotted lines in Fig. 2 are related to input constraint enforcement discussed in Section III-D; they are ignored in all derivations in this section.

A control designer is free to implement H_{ff} and H_{fb} using a wide range of FF and FB controllers (linear or nonlinear) available in the literature. In the rest of this section, we present a sample FF and FB implementation of the proposed allocation scheme. The presented examples are classical controllers which can easily be implemented in real time, with low computational burden. However, the proposed scheme is also amenable to implementation via advanced controllers like H_2/H_∞ control, sliding mode control, and model predictive control.

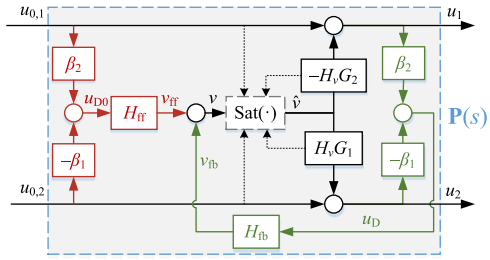

Fig. 2. General structure of proposed allocation approach comprising FF control (H_{ff}), FB control (H_{fb}) and actuator constraint handling [Sat$(\cdot)$].

1) Classical FF Implementation: Focusing on FF control (marked in red in Fig. 2) by setting $H_{\mathrm{fb}} = 0$, $u_{\mathrm{D}} = 0$ requires

$$\beta_2 (u_{0,1} - H_v G_2 v) - \beta_1 (u_{0,2} + H_v G_1 v) = 0$$
$$\Rightarrow v_{\mathrm{ff}} = (H_v (\beta_1 G_1 + \beta_2 G_2))^{-1} u_{\mathrm{D}0} = H_{\mathrm{ff}} u_{\mathrm{D}0}. \tag{23}$$

Note that selecting H_{ff} as defined in (23) may not always be feasible in the presence of non-minimum phase (NMP) zeros in $\beta_1 G_1 + \beta_2 G_2$; moreover, H_{ff} may not be causal. Approximate inversion techniques, like zero phase error tracking controller (ZPETC) [24], zero magnitude error tracking controller (ZMETC) [25], etc., may be used to achieve $u_{\mathrm{D}0} \approx 0$ over certain frequency ranges. Note that these approximate inversion techniques may yield nonproper H_{ff}, which can be addressed via noncausal implementation using future values of $u_{\mathrm{D}0}$ (e.g., portions of $u_{\mathrm{D}0}$ calculated based on known reference command y_{r}) [24]. It can also be addressed by adding fast poles to H_{ff} to make it causal [26], as is demonstrated in Section IV-C.

2) Classical FB Implementation: Focusing on FB control (marked in green in Fig. 2) by setting $H_{\mathrm{ff}} = 0$, we get

$$v_{\mathrm{fb}} = H_{\mathrm{fb}} u_{\mathrm{D}} = H_{\mathrm{fb}} \begin{bmatrix} \beta_2 & -\beta_1 \end{bmatrix} \mathbf{u}. \tag{24}$$

Accordingly, the overall transfer function of $\mathbf{P}$ is given by

$$\begin{bmatrix} u_1 \\ u_2 \end{bmatrix} = \underbrace{\frac{\begin{bmatrix} 1 + \beta_1 H_{\mathrm{fb}} H_v G_1 & \beta_1 H_{\mathrm{fb}} H_v G_2 \\ \beta_2 H_{\mathrm{fb}} H_v G_1 & 1 + \beta_2 H_{\mathrm{fb}} H_v G_2 \end{bmatrix}}{1 + H_{\mathrm{fb}} H_v (\beta_1 G_1 + \beta_2 G_2)}}_{=\mathbf{P}} \begin{bmatrix} u_{0,1} \\ u_{0,2} \end{bmatrix}. \tag{25}$$

The allocator's effect on control alignment with the optimal ratio is evaluated as

$$u_{\mathrm{D}} = \frac{u_{\mathrm{D}0}}{1 + H_{\mathrm{fb}} H_v (\beta_1 G_1 + \beta_2 G_2)}. \tag{26}$$

Here, the allocator's characteristic equation

$$\theta (s) \triangleq 1 + H_{\mathrm{fb}} H_v (\beta_1 G_1 + \beta_2 G_2) \tag{27}$$

is crucial as it determines the allocator performance and stability [20]. FB controller H_{fb} can be shaped to deliver a large norm of θ at targeted frequency ranges where efficiency is most desired, while ensuring system stability (e.g., using classical root locus techniques), as demonstrated in Section IV-C. Note that

even though FF and FB implementations have been discussed separately, they can be combined together, as shown in Fig. 2, to give

$$v = v_{\text{ff}} + v_{\text{fb}} = \frac{(H_{\text{ff}} + H_{\text{fb}})\, u_{\text{D0}}}{1 + H_{\text{fb}} H_v\, (\beta_1 G_1 + \beta_2 G_2)}. \tag{28}$$

D. Actuator Constraint Handling: Assume that u_1 and u_2 have saturation bounds given by

$$U_1^- \le u_1 \le U_1^+, \qquad U_2^- \le u_2 \le U_2^+. \tag{29}$$

As shown in Fig. 2, we seek to enforce these bounds on $\mathbf{u}$ indirectly through v. This can be done by transferring output bounds to input bounds following the technique discussed in [27], [28]. To do this, assume $\mathbf{A}_i$, $\mathbf{B}_i$, $\mathbf{C}_i$, and $\mathbf{D}_i$ $(i = 1, 2)$ with corresponding state vectors $\mathbf{z}_i$, formulate discrete-time realizations of $-H_v G_2$(for $i = 1$) and $H_v G_1$ (for $i = 2$). Both these two state-space discrete systems are assumed to be strictly proper $(\mathbf{D}_i = \mathbf{0})$ to avoid possible algebraic loops. This can be assured by proper choice of H_v. The relative degrees of the two systems r_i, marked by the first nonzero Markov parameters, are each defined as the smallest integer satisfying

$$\mathbf{C}_i \mathbf{A}_i^{r_i - 1} \mathbf{B}_i \neq 0, \quad \mathbf{C}_i \mathbf{A}_i^{t} \mathbf{B}_i = 0\, (t = 0, 1, \ldots, r_i - 2)\,. \tag{30}$$

In other words, relative degree determines the minimum number of time steps needed before a system's input affects its output. With relative degree r_i, only constraints associated with $\mathbf{u}[t + r_i]$ and beyond can be enforced by $v[t]$ for a given $\mathbf{z}_i[t]$, i.e.

$$U_i^- \le \mathbf{C}_i \mathbf{A}_i^{r_i} \mathbf{z}_i\,[t] + \mathbf{C}_i \mathbf{A}_i^{r_i - 1} \mathbf{B}_i v\,[t] + u_{0,i}\,[t + r_i] \le U_i^+. \tag{31}$$

Assuming that the fluctuation of $u_{0,i}$ is negligible within r_i time steps (i.e., $u_{0,i}[t] \approx u_{0,i}[t+1] \cdots \approx u_{0,i}[t + r_i]$), we can write

$$U_i^- - u_{0,i} - \mathbf{C}_i \mathbf{A}_i^{r_i} \mathbf{z}_i \le \left(\mathbf{C}_i \mathbf{A}_i^{r_i - 1} \mathbf{B}_i\right) v \le U_i^+ - u_{0,i} - \mathbf{C}_i \mathbf{A}_i^{r_i} \mathbf{z}_i. \tag{32}$$

Accordingly, the limits on $\mathbf{u}$ can be indirectly satisfied by imposing constraints on v as

$$\begin{aligned} \underline{v} &= \max_{i=1,2} \left(\mathbf{C}_i \mathbf{A}_i^{r_i - 1} \mathbf{B}_i\right)^{-1} \left[U_i^{-\alpha_i} - u_{0,i} - \mathbf{C}_i \mathbf{A}_i^{r_i} \mathbf{z}_i\right] \\ \bar{v} &= \min_{i=1,2} \left(\mathbf{C}_i \mathbf{A}_i^{r_i - 1} \mathbf{B}_i\right)^{-1} \left[U_i^{\alpha_i} - u_{0,i} - \mathbf{C}_i \mathbf{A}_i^{r_i} \mathbf{z}_i\right] \\ \alpha_i &\triangleq \operatorname{sgn}\left(\mathbf{C}_i \mathbf{A}_i^{r_i - 1} \mathbf{B}_i\right) \end{aligned} \tag{33}$$

where $\underline{v}$ and $\bar{v}$, respectively, denote the lower and upper bounds on v; α_i is the sign of the first nonzero Markov parameter. Accordingly, the saturation function in Fig. 2 is defined as [28]

$$\hat{v} = \operatorname{sat}\,(v, \underline{v}, \bar{v}) = \max\left(\min\left(\underline{v}, \bar{v}\right), \min\left(v, \max\left(\underline{v}, \bar{v}\right)\right)\right). \tag{34}$$

Notice from (33) that $\underline{v}$ and $\bar{v}$ are, respectively, determined by selecting the greater and the smaller value of constraints on v associated with u_1 and u_2. There is, however, no guarantee that $\underline{v}$ is always smaller than $\bar{v}$, meaning that it may be infeasible for v to lie between $\underline{v}$ and $\bar{v}$. This situation is likely to occur when the dynamics or constraints associated with u_1 and u_2 are very different from each other, especially when high-frequency dynamics are considered [28]. High-frequency dynamics also makes it difficult to satisfy the assumption that $u_{0,i}[t] \approx u_{0,i}[t+1] \cdots \approx u_{0,i}[t + r_i]$. In practice, these issues can be greatly mitigated by using only the low frequency portion of $\mathbf{u}_0$ in (33) and selecting pre-filter H_v as a low-pass filter to attenuate high-frequency dynamics outside the desired allocator bandwidth. The implication is that the Sat$(\cdot)$ block imposes constraints on low-frequency dynamics, but not necessarily on high-frequency dynamics, as is illustrated in Section IV-D.

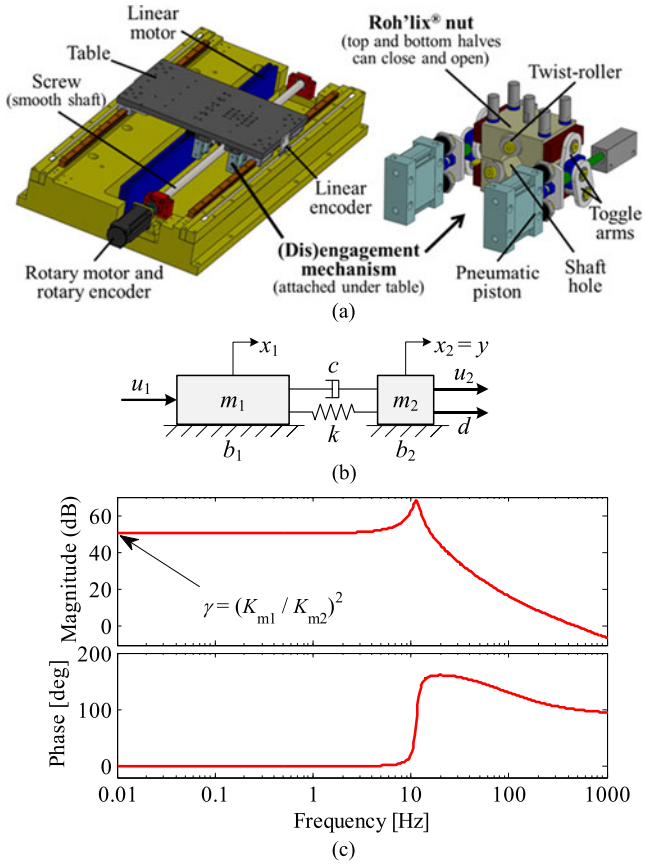

Fig. 3. (a) HFD with (dis)engagement mechanism, (b) two-mass model of HFD, and (c) optimal control ratio of HFD.

IV. Validation on Over-Actuated Hybrid Feed Drive

A. Overview of Hybrid Feed Drive

Fig. 3(a) shows a schematic of the dual-input over-actuated precision servo positioner used in this paper to evaluate the proposed control allocation method. It is a hybrid feed drive (HFD) [29] consisting of a linear motor, and a rotary motor which generates single DOF linear motion through screw action via a reconfigurable Roh'lix nut [30]. The Roh'lix nut (which comes in two spring-loaded halves) acts as a clutch that can be opened to disengage from the shaft, allowing the linear motor to act alone (during rapid motion). It can equally be closed to engage with the shaft such that the linear motor and rotary motor can work in tandem to generate linear motion during cutting (e.g., milling).

TABLE I
EXPERIMENTALLY IDENTIFIED PARAMETERS OF HFD'S TWO-MASS MODEL

m_1 (kg)	616.2	b_1 (kg/ s)	44.8	$K_{m1}(N/\sqrt{W})$	380.8
m_2 (kg)	46.3	b_2 (kg/ s)	83.3	$K_{m2}(N/\sqrt{W})$	21
c (kg/ s)	5777.2	k (N/μm)	3.147	γ	328.8

Prior work [29] has demonstrated superior precision and significant improvements in efficiency (compared to a linear motor) as a result of the over-actuation of the HFD in its cutting mode. To achieve high precision and efficiency using the HFD, the right balance must be struck between actuation by the linear and rotary motors. The rotary motor is more energy efficient, while the linear motor provides higher system bandwidth due to its collocated placement with the output (i.e., table's position). The objective of control allocation for the HFD is to improve efficiency without sacrificing table positioning performance. This requires a broadband allocation scheme due to the difference in efficiency and bandwidth of the two actuators.

B. Modeling of Hybrid Feed Drive

Similar to [18], the HFD is modeled, as shown in Fig. 3(b), as a simple two-mass system described by the equations

$$\begin{aligned} m_1\ddot{x}_1 + b_1\dot{x}_1 + c(\dot{x}_1 - \dot{x}_2) + k(x_1 - x_2) &= u_1 \\ m_2\ddot{x}_2 + b_2\dot{x}_2 + c(\dot{x}_2 - \dot{x}_1) + k(x_2 - x_1) &= u_2 + d \end{aligned} \tag{35}$$

where m_1 represents the equivalent mass of the rotor and shaft; m_2 is the mass of the table; x_1 and x_2 are the displacements of the two masses, with $y = x_2$ being the target for precision control; k, c, b_1, b_2 are stiffness, damping terms [see Fig. 3(b)]; d is the disturbance force (dominated by cutting forces applied to the table); u_1 and u_2 are the equivalent input forces to the two-mass system. The experimentally identified parameters [18] of the HFD's two-mass model are shown in Table I. In transfer function format

$$\begin{aligned} y = x_2 &= \begin{bmatrix} G_1 & G_2 \end{bmatrix} \begin{bmatrix} u_1 & u_2 \end{bmatrix}^T + G_2 d \\ G_1 &= \frac{G_{1n}}{D_{ol}}, \quad G_2 = \frac{G_{2n}}{D_{ol}} \\ G_{1n} &= cs + k, \quad G_{2n} = m_1 s^2 + (c + b_1)\, s + k \\ D_{ol} &= a_{ol,4} s^4 + a_{ol,3} s^3 + a_{ol,2} s^2 + a_{ol,1} s \\ a_{ol,4} &= m_1 m_2, \quad a_{ol,3} = b_1 m_2 + b_2 m_1 + c\,(m_1 + m_2) \\ a_{ol,2} &= c\,(b_1 + b_2) + k\,(m_1 + m_2) + b_1 b_2 \\ a_{ol,1} &= (b_1 + b_2)\, k. \end{aligned} \tag{36}$$

The control energy cost functional (i.e., thermal loss) for the HFD is modeled as the heat generated by its actuators during operation, i.e.

$$J = \int \left(\left(\frac{u_1}{K_{m1}} \right)^2 + \left(\frac{u_2}{K_{m2}} \right)^2 \right) dt \tag{37}$$

where K_{m1} and K_{m2} (shown in Table I) are the motor constants of the rotary and linear motor, respectively. They each represent the efficiency of corresponding actuator, and ratio $\gamma = (K_{m1}/K_{m2})^2$ represents the energy optimal static control ratio. Notice that (37) follows the general quadratic format in (5), with $R_{11} = (1/K_{m1})^2$, $R_{22} = (1/K_{m2})^2$, $R_{12} = 0$. Accordingly, the HFD's optimal control ratio and its factorization are given by

$$\begin{aligned} \beta^* &= \frac{K_{m1}^2}{K_{m2}^2} \frac{k - cs}{m_1 s^2 - (c + b_1)\, s + k} = \frac{\beta_1}{\beta_2} \\ \beta_1 &= \frac{k - cs}{K_{m2}^2 \psi}, \quad \beta_2 = \frac{m_1 s^2 - (c + b_1)\, s + k}{K_{m1}^2 \psi}. \end{aligned} \tag{38}$$

Accordingly Π and ψ are determined (based on $\psi^* \psi = \Pi$) as

$$\begin{aligned} \Pi &= \frac{{m_1}^2 s^4 + \left(2m_1 k - (c + b_1)^2 - \gamma c^2 \right) s^2 + (\gamma + 1)\, k^2}{K_{m1}^2} \\ &= \underbrace{\left[\frac{m_1 s^2 - a_{\psi 1} s + a_{\psi 0}}{K_{m1}} \right]}_{\psi^*} \underbrace{\left[\frac{m_1 s^2 + a_{\psi 1} s + a_{\psi 0}}{K_{m1}} \right]}_{\psi} \end{aligned} \tag{39}$$

where

$$\begin{aligned} a_{\psi 1} &= \sqrt{2m_1 k \sqrt{(1 + \gamma)} - 2m_1 k + (c + b_1)^2 + \gamma c^2} \\ a_{\psi 0} &= k \sqrt{(1 + \gamma)}. \end{aligned} \tag{40}$$

It can be verified that β_1 and β_2 are causal stable, with poles at $-226 \pm 204j$ rad/ s.

Fig. 3(c) shows the Bode plot of β^*. Notice, according to (38), that β^* combines the actuators' frequency dependent maneuverability with their energy cost. At low frequencies, $\beta^* \to \gamma$, as in static-model-based dynamic allocation methods [15], indicating that the rotary motor is preferred for efficiency. However, at higher frequencies, $\beta^* \to 0$, indicating that it is more efficient to utilize the linear motor for precision positioning, since the rotary motor loses control of the table at high frequencies due to the mechanical decoupling effect in two-mass system with noncollocated input and output [31]. This frequency dependent change in optimal ratio requires broadband allocation, which cannot be achieved with static-model-based dynamic allocation methods. Notice the positive phase of β^* at resonance and beyond, indicating that it is unstable hence not causally implementable.

C. Design of Nominal Controller and Control Allocator

1) Design of Nominal Controller: Let us assume that the HFD is required to track a broadband snap-limited reference position signal y_r, whose velocity profile is shown in Fig. 4(a) and kinematic limits are given in Table II. Moreover, as shown in Fig. 4(b), during the constant velocity portion of y_r, from 1 to 4.5 s, the HFD must reject disturbance force d, given by

$$d = \underbrace{100 \cos(20\pi t) - 100}_{\text{Dominant}} + \underbrace{H_d N(0, \sigma^2)}_{\text{Nondominant}} \text{N} \tag{41}$$

representing cutting force disturbance with a dominant dc and harmonic portion (at 10 Hz), combined with a nondominant broadband portion made up of zero-mean white noise with stan-

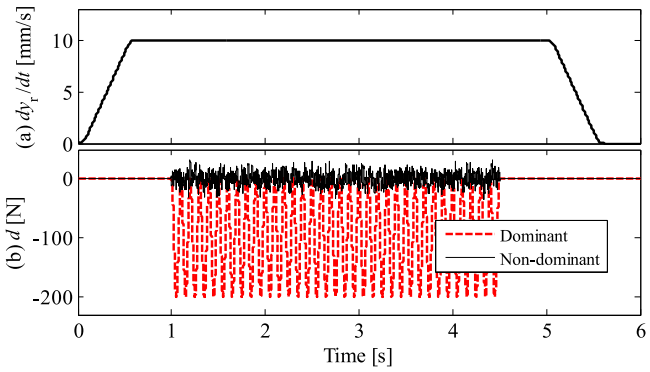

Fig. 4. (a) Velocity reference command and (b) disturbance force profiles.

TABLE II
KINEMATIC LIMITS OF REFERENCE TRAJECTORY AND PID CONTROLLER GAINS

Pos. (mm)	Vel. (mm/s)	Acc. (mm/s^2)	Jerk (mm/s^3)	Snap (mm/s^4)
5	10	20	200	1×10^4
K_p (N/m)	K_i (N $\cdot$ m$^{-1}\cdot$s^{-1})	K_d (N $\cdot$ m$^{-1}\cdot$s^{-1})		T_f (s)
7.46×10^6	4.07×10^6	1.01×10^5		1.39×10^{-4}

dard deviation $\sigma = 100$ N, low-pass filtered with H_d given by

$$H_d = \frac{\omega_d}{s + \omega_d}. \tag{42}$$

Here, $\omega_d = 60\,\pi$ rad/ s is employed such that the low-pass filter has cutoff frequency of 30 Hz.

The nominal controller (i.e., $\mathbf{C}$ in Fig. 1) is designed with an FF component ($\mathbf{C}_{\rm ff}$) for reference tracking and a FB component ($\mathbf{C}_{\rm fb}$) for regulation such that $\mathbf{u}_0 = \mathbf{u}_{\rm ff0} + \mathbf{u}_{\rm fb0}$.

The FF controller can be designed as

$$\mathbf{u}_{\rm ff0} = \mathbf{C}_{\rm ff}\, y_{\rm r} = \begin{bmatrix} m_1 s^2 + b_1 s \\ m_2 s^2 + b_2 s \end{bmatrix} y_{\rm r} \tag{43}$$

which is the simplest FF controller for achieving perfect tracking of $y_{\rm r}$; it forces the two-mass HFD to move as one rigid body [18], [32].

The FB controller is designed as a proportional-integral-derivative (PID) controller given by

$$\mathbf{u}_{\rm fb0} = \mathbf{C}_{\rm fb}\,(y_{\rm r} - y) = \begin{bmatrix} 0 \\ K_p + \dfrac{K_i}{s} + \dfrac{K_d s}{T_f s + 1} \end{bmatrix} (y_{\rm r} - y) \tag{44}$$

where K_p, K_i, K_d, T_f are calculated using MATLAB's PID tuning tool targeted at a crossover frequency of 10 Hz, and their values are provided in Table II. Notice that $\mathbf{C}_{\rm fb}$ uses only $y = x_2$ for FB and only u_2 for actuation (i.e., single-input single-output collocated control) which makes for ease of design. Moreover, neither the FF nor FB controller is designed with efficiency in mind; they both rely on the control allocator to deal with efficiency. This demonstrates the elegance of the two-stage framework upon which the proposed allocator is built.

2) Design of Proposed Energy Optimal Control Allocator: The proposed allocator is designed using the classical FF and FB implementations discussed in Section III-C. The FB allocator ($H_{\rm fb}$) is designed to make $u_{\rm D} \approx 0$ at 0 and 10 Hz, corresponding to the frequencies of the dominant components of d, which are often known in practical milling scenarios and are most critical to precision and control energy [18]. The FF allocator ($H_{\rm ff}$) is designed to yield $u_{\rm D} \approx 0$ in a broadband sense, to provide allocation for portions of u_0 induced by $y_{\rm r}$ and the broadband portion of d. The prefilter H_v is given by

$$H_v\,(s) = D_{\rm ol}\,(s)/\,D_{\rm d}\,(s) \tag{45}$$

which replaces the denominator of the original system $D_{\rm ol}$ containing undesirable structural modes, with a more desirable denominator $D_{\rm d}$. Here, $D_{\rm d}$ is selected as a third-order Butterworth low-pass filter with cutoff frequency of 16 Hz, corresponding to the target bandwidth of the allocator (which is greater than the 10 Hz crossover frequency of $\mathbf{C}_{\rm fb}$). The numerator of $D_{\rm d}$ is scaled with stiffness k (which is the dc gain of $G_{1\rm n}$ and $G_{2\rm n}$) so that the v has force unit (N).

The FB allocator $H_{\rm fb}$ is selected as

$$H_{\rm fb}\,(s) = K_{\rm AL} W_d\,(s) \tag{46}$$

where $K_{\rm AL}$ is a gain which selected to make $\theta(s)$ in (27) as high as possible; W_d is a weighting filter that emphasizes frequencies where high $\theta(s)$ is most desirable, since, due to stability constraints, it is impossible to make $\theta(s)$ very high at all frequencies. We select

$$W_d\,(s) = \frac{1}{s + \varepsilon} \cdot \frac{{\omega_0}^2}{s^2 + 2\zeta\omega_0 s + {\omega_0}^2} \tag{47}$$

with $\omega_0 = 20\pi$ rad/ s (i.e., 10 Hz), so that W_d magnifies $\theta(s)$ at the dominant frequencies contained in d. Note that $\varepsilon = 10^{-5}$ rad/ s and $\zeta = 0.01$ are introduced to ensure very high gains at the desired frequencies while keeping the energy of W_d finite. By treating $W_d H_v(\beta_1 G_1 + \beta_2 G_2)$ as an open loop plant, the standard root locus technique is used to determine $K_{\rm AL} = 270$ N/$\sqrt{W}$ as a high enough FB gain that ensures closed loop stability. Fig. 5(a) shows the root locus and final closed loop poles of allocator $\mathbf{P}$ (i.e., the roots of $\theta(s)$).

According to (23), FF allocator, $H_{\rm ff}$, is given by

$$H_{\rm ff} = \left(H_v(\beta_1 G_1 + \beta_2 G_2)\right)^{-1} = \frac{D_{\rm d}\,(s)}{\psi^*\,(s)}. \tag{48}$$

However, the expression $\psi^*(s) = \psi(-s)$ in the denominator of $H_{\rm ff}$ has unstable poles [see (39)]. Moreover, $H_{\rm ff}$ is nonproper and hence noncausal. An approximation of $H_{\rm ff}$ based on ZPETC [24] is given by

$$H_{\rm ff\_ZPETC} = \frac{\psi\,(s)\,D_{\rm d}\,(s)}{\psi(0)^2} H_0\,(s) \tag{49}$$

where H_0 is a sixth-order Butterworth low-pass filter (similar to the inverse compensation filter [26]) added to make $H_{\rm ff\_ZPETC}$ causal.

As discussed in Section III-C, the FF and FB implementations of the proposed allocator can be employed independently, or combined. In Fig. 5(b), the frequency spectra of

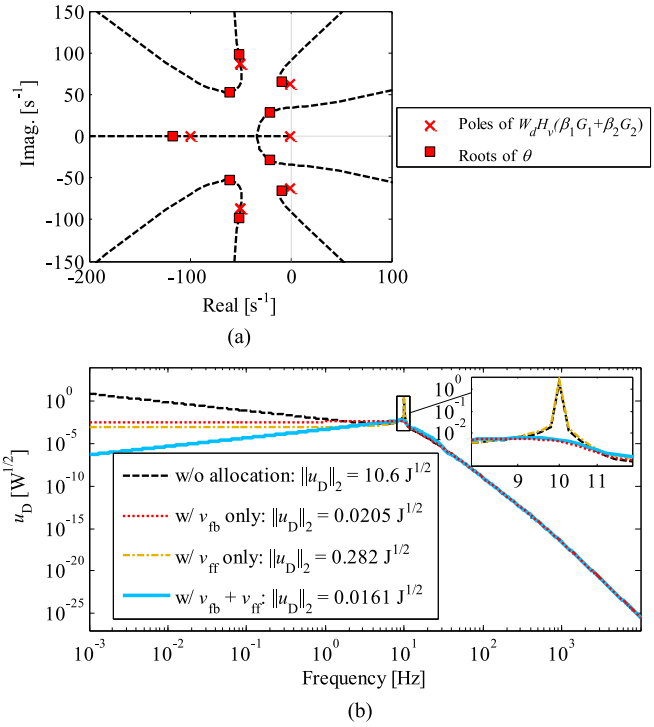

Fig. 5. (a) Root locus plot of FB allocator. (b) Comparison of estimated frequency spectra of u_D achieved without allocation and with the proposed FF and/or FB allocators.

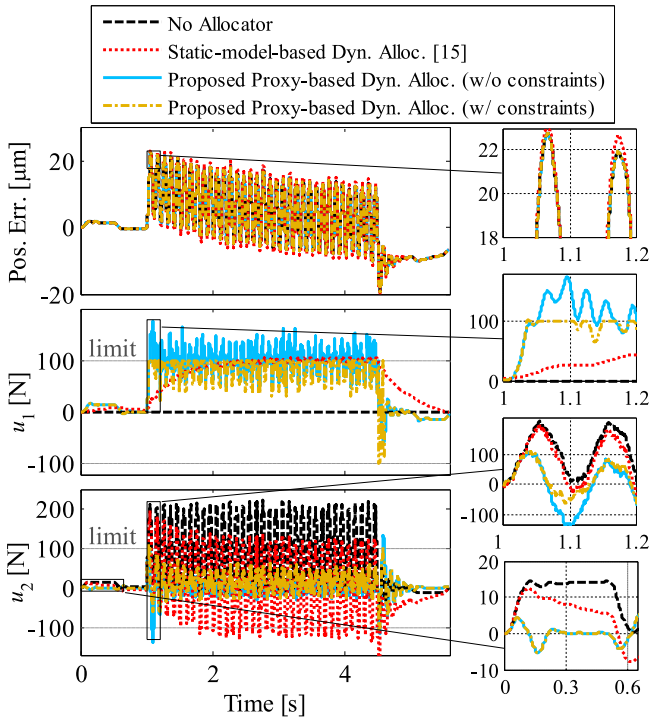

Fig. 6. Time-domain comparison of positioning performance and control efforts of allocation methods (simulation).

u_D for different implementations are compared by substituting $d(s) \approx W_d(s)$ and $y_r = 0$ in closed-loop system transfer functions (i.e., by focusing on the dominant portions of d). Notice that, without allocation, u_D inherits the high dc gain and peak at 10 Hz, corresponding to the dominant portions of d, resulting in $||u_D||_2 = 10.6\sqrt{\text{J}}$. The FB allocator eliminates the 10 Hz peak and flattens out the dc gain of u_D such that $||u_D||_2 = 0.0205\sqrt{\text{J}}$. The FF allocator reduces u_D (more than achieved by the FB allocator) for frequencies up to 10 Hz, but is not as effective as the FB allocator in suppressing the 10 Hz peak; the result is $||u_D||_2 = 0.282\sqrt{\text{J}}$. The combination of both FB and FF allocators does the best job of reducing u_D in a broadband sense, including the 10 Hz peak, resulting in $||u_D||_2 = 0.0161\sqrt{\text{J}}$. Therefore, the combination of FF and FB designs is employed in comparing the proposed allocator to an existing allocator in the following section.

D. Simulation and Experiment Results

In this section, the proposed proxy-based (PB) dynamic allocator designed in Section IV-C is compared to the static-model-based (SMB) dynamic allocator by Zaccarian [15], which circumvents time consuming real-time optimization by approximating (2) as

$$\text{Ker}\left(\lim_{s\to 0}\mathbf{G}(s)\right) \neq \varnothing. \tag{50}$$

In other words, it considers weak redundancy only in a static sense. The SMB allocator is implemented as detailed in [15] based on the parameters of the HFD, and with energy performance matrix $\bar{W} = \text{diag}(K_{m1}^{-2},\ K_{m2}^{-2})$ and allocator speed parameter $K = 10^3$.

TABLE III
POSITIONING PERFORMANCE AND AVERAGE CONTROL POWER CONSUMPTION COMPARISON (SIMULATION)

	Pos. Err. (μm)		Control Power (W)		
	Max.	RMS	P_1	P_2	P_{total}
No Allocator	22.73	8.96	0	21.982	21.982
SMB Allocator [15]	23.08	9.41	0.038	11.092	11.130
Proposed PB Allocator (w/o constraints)	22.73	8.96	0.047	1.108	1.155
Proposed PB Allocator (w/ constraints)	22.73	8.96	0.034	1.396	1.430

1) Simulation Results: The nominal FF and FB controllers designed in Section III-C are applied to both the PB and the SMB allocator; both allocators are benchmarked against the nominal controller with no allocator, regarding positioning error and control power (i.e., control energy in unit time). Also, in order to illustrate the constraint-handling approach proposed in Section III-D, an additional case with saturation limits $U_1^{\pm} = U_2^{\pm} = \pm 100$ N applied to the PB allocator is simulated. The inputs to the simulation are y_r and d given in Fig. 4.

As shown in the tracking results of Fig. 6, and statistics reported in Table III, relative to the no allocator case, the SMB allocator introduces 2% and 5% more maximum and root mean square (RMS) tracking errors, respectively. However, the proposed PB allocator (with and without constraints) preserves the

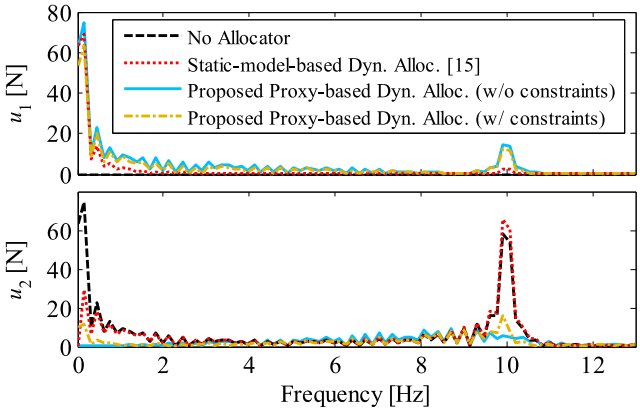

Fig. 7. Comparison of control effort frequency spectra of allocation methods (simulation).

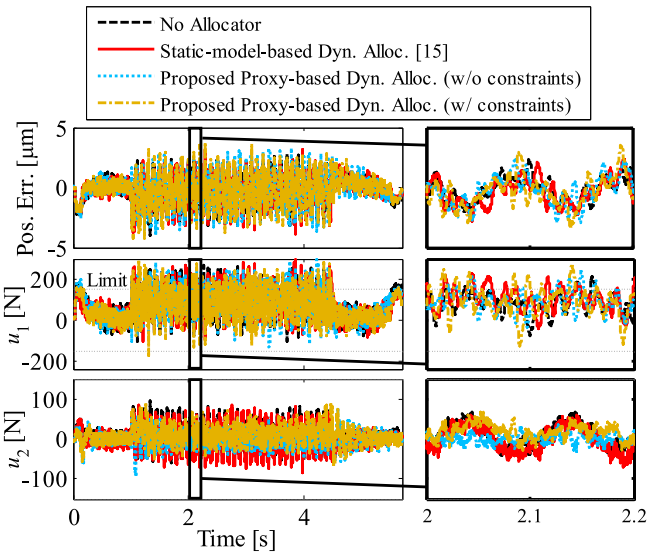

Fig. 8. Time-domain comparison of positioning performance and control efforts of allocation methods (experiment).

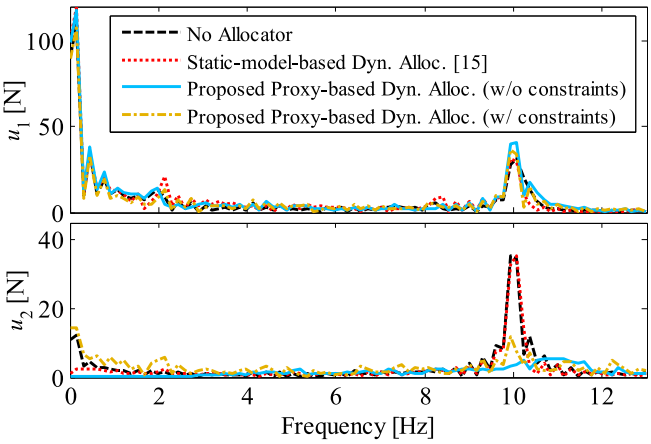

Fig. 9. Comparison of control effort frequency spectra of allocation methods (experiment).

tracking performance perfectly. Notice from Fig. 6 that, as expected, the PB and SMB allocators both re-assign more of the static control effort to the more-efficient rotary motor, compared to the no-allocator case, which relies heavily on the less-efficient linear motor. The major difference between the SMB allocator and the PB allocator lies at higher frequencies. For instance, in keeping with β^* [see Fig. 3(c)], the PB allocator assigns much more regulation of the 10 Hz disturbance signal to the rotary motor, as shown in Figs. 6 and 7; the SMB allocator does not. As a result, without constraints imposed, the PB allocator, respectively, consumes 95% and 90% less average control power than the no allocator and the SMB allocator cases. Fig. 6 also illustrates the effectiveness of the constraint-handling approach discussed in Section III-D, applied to the PB allocator; notice that it truncates the portions of u_1 that exceed the imposed limits and reassigns them to u_2. This reassignment does not affect positioning performance, because, as shown in Fig. 2, it occurs in the null space of $\mathbf{G}$. However, the reassignment violates the requirements of β^*, resulting in 24% more average control power consumption compared to the unconstrained case. Nonetheless, even with constraints imposed, the proposed PB allocator still significantly outperforms the no allocator and SMB allocator cases.

2) Experiment Results: The proposed PB allocation approach is evaluated in experiments conducted on an in-house-built prototype of the HFD of Fig. 3(a) (see [28] for details), controlled at 10 kHz sampling frequency using dSPACE DS1103 control board. The same FF controller used in the simulations, combined with a PPI–proportional-derivative (PD) controller reported in [33], is used as the nominal FB controller in the experiments. The PPI–PD controller controls the rotary and linear motors using a PPI and a PD controller, respectively, and is optimized for positioning performance using an H_∞ approach [33]. Even though its design is more involved, it achieves higher bandwidth (107 Hz) and is heuristically more efficient than the PID control approach used in simulations—because it applies the integrator to the rotary motor rather than to the linear motor. The exact same reference command, disturbance forces, SMB allocator [15], and FF+FB implementations of proposed PB allocator as used in simulations are adopted in the experiments; the disturbance forces are applied to the table via the linear motor. An additional case with saturation limits of $U_1^{\pm} = U_2^{\pm} = \pm 150$ N is considered. The control signals are low-pass filtered with cutoff frequency of 100 Hz before passing them to the constraint handler to avoid issues with high-frequency control signals, as discussed in Section III-D.

The time-domain and frequency-domain results from the experiments are shown in Figs. 8 and 9, and the tracking error and average control power statistics are reported in Table IV. Unlike in the simulations, in the experiments, the tracking errors of the proposed PB allocator are slightly higher compared to those of the nominal controller. This is because the PB allocator, being model based, can only guarantee invariance of control performance in the absence of modeling errors, which is not the case in the experiments. From energy point of view, the SMB allocator [15] consumes only 2% less average control power than the no allocator case, due to the more-efficient nominal controller

TABLE IV
POSITIONING PERFORMANCE AND AVERAGE CONTROL POWER CONSUMPTION COMPARISON (EXPERIMENTS)

	Pos. Err. (μm)		Control Power (W)		
	Max.	RMS	P_1	P_2	P_{total}
No Allocator	4.02	1.04	0.065	2.016	2.081
SMB Allocator [15]	3.94	1.02	0.068	1.964	2.031
Proposed PB Allocator (w/o constraints)	3.98	1.20	0.072	1.055	1.127
Proposed PB Allocator (w/ constraints)	4.19	1.12	0.062	1.472	1.534

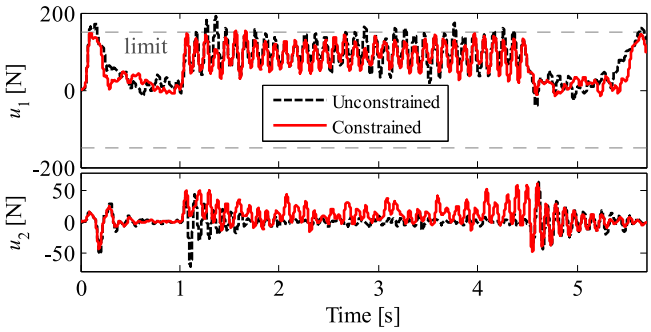

Fig. 10. Comparison of control efforts of proposed proxy-based dynamic allocator with and without constraints, low-pass filtered with 16 Hz cutoff.

adopted in the experiments. However, for the same reasons, as discussed in the simulations, without constraints, the proposed PB allocator consumes 45% and 24% less control power than the SMB allocator, without and with constraints imposed, respectively. Notice from Fig. 8 that even with constraints imposed, u_1 appears to violate the constraints. The reason is that, as explained in Section III-D, the constraint handler does not impose constraints on signals above the allocator bandwidth regulated by H_v (16 Hz). Fig. 10 compares the control signals of Fig. 8 for the proposed allocator with and without constraints, filtered using a low-pass filter with 16 Hz cutoff frequency. Notice that, as expected, the constraint handler redistributes the control effort from u_1 to u_2 to satisfy the constraints. The constraint handler is thus suitable for many practical applications where constraint violation by high-frequency portions of signals is not a major concern.

V. CONCLUSION AND FUTURE WORK

An elegant method for energy optimal dynamic control allocation for dual-input, single-output over-actuated systems is proposed. An optimal control ratio is defined, representing the relationship between two control inputs to ensure control energy optimality without sacrificing performance (i.e., without altering a desired output). However, the optimal control ratio is in general noncausally implementable due to stability issues. Through factorization, a causal and stable deviation measure from the optimal control ratio is derived. The deviation measure is shown to be an accurate proxy for deviation from control energy optimality. Hence, the proposed proxy-based dynamic allocation approach drives the control system to control energy optimality by regulating the deviation measure using classical or advanced FF or FB controllers. Due to their simplicity and the fact that they do not require real-time optimization, classical FF and FB implementations of the proposed proxy-based allocation approach are discussed. A method for handling actuator constraints without sacrificing performance is also presented. The proposed proxy-based dynamic allocation approach is compared to an existing static-model-based dynamic allocator in simulations and experiments on an over-actuated hybrid feed drive. Large improvements in efficiency without sacrificing performance are demonstrated. The effectiveness of the constraint handler on imposing constraints on low-frequency portions of control signals is also shown. Future work will generalize the proposed allocation approach to multi-input multi-output over-actuated systems with more general cost functions and constraints. Issues of robustness to model uncertainty/mismatch will also be rigorously addressed.

REFERENCES

[1] M. G. E. Schneiders, M. J. G. Van De Molengraft, and M. Steinbuch, "Benefits of over-actuation in motion systems," in *Proc. 2004 Amer. Control Conf.*, 2004, vol. 1, pp. 505–510.
[2] J. Zheng, W. Su, and M. Fu, "Dual-stage actuator control design using a doubly coprime factorization approach," *IEEE/ASME Trans. Mechatronics*, vol. 15, no. 3, pp. 339–348, Jun. 2010.
[3] M. J. C. Ronde, M. G. E. Schneiders, E. J. G. J. Kikken, M. J. G. van de Molengraft, and M. Steinbuch, "Model-based spatial feedforward for over-actuated motion systems," *Mechatronics*, vol. 24, no. 4, pp. 307–317, Jun. 2014.
[4] P. A. Servidia and R. S. Pena, "Spacecraft thruster control allocation problems," *IEEE Trans. Autom. Control*, vol. 50, no. 2, pp. 245–249, Feb. 2005.
[5] Y. Chen and J. Wang, "Adaptive energy-efficient control allocation for planar motion control of over-actuated electric ground vehicles," *IEEE Trans. Control Syst. Technol.*, vol. 22, no. 4, pp. 1362–1373, Jul. 2014.
[6] K. Tagesson, P. Sundstrom, L. Laine, and N. Dela, "Real-time performance of control allocation for actuator coordination in heavy vehicles," in *Proc. 2009 IEEE Intell. Veh. Symp.*, 2009, pp. 685–690.
[7] R. Brinkerhoff and S. Devasia, "Output tracking for actuator deficient/redundant systems: Multiple piezoactuator example," *J. Guid. Control. Dyn.*, vol. 23, no. 2, pp. 370–373, Mar. 2000.
[8] Y. Halevi, E. Carpanzano, and G. Montalbano, "Minimum energy control of redundant linear manipulators," *J. Dyn. Syst. Meas. Control*, vol. 136, no. 5, p. 51016, Jul. 2014.
[9] H. Cheng, Y.-K. Yiu, and Z. Li, "Dynamics and control of redundantly actuated parallel manipulators," *IEEE/ASME Trans. Mechatronics*, vol. 8, no. 4, pp. 483–491, Dec. 2003.
[10] T. A. Johansen and T. I. Fossen, "Control allocation—A survey," *Automatica*, vol. 49, no. 5, pp. 1087–1103, May 2013.
[11] O. Härkegård and S. T. Glad, "Resolving actuator redundancy—optimal control vs. control allocation," *Automatica*, vol. 41, no. 1, pp. 137–144, Jan. 2005.
[12] O. Härkegård, "Dynamic control allocation using constrained quadratic programming," *J. Guid. Control. Dyn.*, vol. 27, no. 6, pp. 1028–1034, Nov. 2004.
[13] J. A. M. Petersen and M. Bodson, "Constrained quadratic programming techniques for control allocation," *IEEE Trans. Control Syst. Technol.*, vol. 14, no. 1, pp. 91–98, Jan. 2006.
[14] M. Bodson, "Evaluation of optimization methods for control allocation," *J. Guid. Control. Dyn.*, vol. 25, no. 4, pp. 703–711, Jul. 2002.
[15] L. Zaccarian, "Dynamic allocation for input redundant control systems," *Automatica*, vol. 45, no. 6, pp. 1431–1438, Jun. 2009.
[16] J. Zhou, M. Canova, and A. Serrani, "Predictive inverse model allocation for constrained over-actuated linear systems," *Automatica*, vol. 67, pp. 267–276, May 2016.

[17] S. Galeani, A. Serrani, G. Varano, and L. Zaccarian, "On input allocation-based regulation for linear over-actuated systems," *Automatica*, vol. 52, no. 2015, pp. 346–354, Feb. 2015.
[18] M. Duan and C. E. Okwudire, "Energy-efficient controller design for a redundantly actuated hybrid feed drive with application to machining," *IEEE/ASME Trans. Mechatronics*, vol. 21, no. 4, pp. 1822–1834, Aug. 2016.
[19] M. Duan and C. E. Okwudire, "Correction to 'Energy-efficient controller design for a redundantly-actuated hybrid feed drive with application to machining,"' *IEEE/ASME Trans. Mechatronics*, vol. 21, no. 6, pp. 2999–3000, Dec. 2016.
[20] M. Duan and C. E. Okwudire, "Near energy optimal control allocation for dual-input over-actuated systems," in *Proc. ASME 2016 Dyn. Syst. Control Conf.*, 2016, p. V001T01A011.
[21] R. F. Curtain and H. Zwart, *An Introduction to Infinite-Dimensional Linear Systems Theory*, vol. 21, New York, NY, USA: Springer, 2012.
[22] L. Komzsik, *Applied Calculus of Variations for Engineers*, Boca Raton, FL, USA: CRC Press, 2014.
[23] M. V. Kothare and M. Morari, "Multiplier theory for stability analysis of anti-windup control systems," *CDS Technical Report No. CIT/CDS 96-012*, California Institute of Technology, 1996.
[24] M. Tomizuka, "Zero phase error tracking algorithm for digital control," *J. Dyn. Syst. Meas. Control*, vol. 109, no. 1, p. 65, Mar. 1987.
[25] J. A. Butterworth, L. Y. Pao, and D. Y. Abramovitch, "Analysis and comparison of three discrete-time feedforward model-inverse control techniques for nonminimum-phase systems," *Mechatronics*, vol. 22, no. 5, pp. 577–587, Aug. 2012.
[26] M. Weck and G. Ye, "Sharp corner tracking using the IKF control strategy," *CIRP Ann. Manuf. Technol.*, vol. 39, no. 1, pp. 437–441, Jan. 1990.
[27] O. J. Rojas and G. C. Goodwin, "A simple antiwindup strategy for state constrained linear control," in *Proc. IFAC World Congr.*, vol. 35, no. 1, 2002, pp. 109–114.
[28] E. Chambon, L. Burlion, and P. Apkarian, "Time-response shaping using output to input saturation transformation," *Int. J. Control*, vol. 91, no. 3, pp. 534–553, Mar. 2018.
[29] C. Okwudire and J. Rodgers, "Design and control of a novel hybrid feed drive for high performance and energy efficient machining," *CIRP Ann. Manuf. Technol.*, vol. 62, no. 1, pp. 391–394, Jan. 2013.
[30] "Roh'Lix linear actuators," 2013. [Online]. Available: https://www.zero-max.com/ce-rohlix-linear-actuators. Accessed on: Feb. 08, 2018.
[31] R. M. Schmidt, G. Schitter, and A. Rankers, *The Design of High Performance Mechatronics: High-Tech Functionality by Multidisciplinary System Integration*. Amsterdam, Netherlands: IOS Press, 2014.
[32] P. Lambrechts, M. Boerlage, and M. Steinbuch, "Trajectory planning and feedforward design for electromechanical motion systems," *Control Eng. Pract.*, vol. 13, no. 2, pp. 145–157, Feb. 2005.
[33] M. Duan and C. E. Okwudire, "Energy efficiency and performance optimized control of a hybrid feed drive," in *Proc. ASME 2015 Int. Manuf. Sci. Eng. Conf.*, 2015, p. V002T05A007.

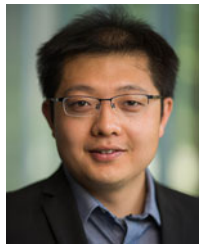

Molong Duan (S'14) received the B.S. degree in theoretical and applied mechanics from Peking University, Beijing, China, in 2012, and the M.S.E. degree from the University of Michigan (U-M), Ann Arbor, MI, USA, in 2013, where he is currently working toward the Ph.D. degree in mechanical engineering.

His current research interests include control of hybrid and redundantly actuated systems, sustainable manufacturing, and intelligent motion command generation.

Mr. Duan was granted the Rackham Centennial Fellowship from U-M in 2013. He received the Best Poster Award at the 2014 International Forum on Sustainable Manufacturing, and the Best Student Paper Award at the 2015 Dynamic Systems and Controls Conference.

Chinedum E. Okwudire (M'15) received the Ph.D. degree in mechanical engineering from the University of British Columbia, Vancouver, BC, Canada, in 2009.

He joined the Mechanical Engineering Faculty with the University of Michigan, Ann Arbor, MI, USA, in 2011. Prior to joining Michigan, he was the Mechatronic Systems Optimization Team Leader at DTL (Mori Seiki, Ltd.), Davis, CA, USA. His expertise lies in smart and sustainable automation, where he leverages the fundamental engineering disciplines of machine design, structural dynamics, and control theory to tackle challenging problems in precision, throughput, and energy efficiency faced by the manufacturing and vehicle automation industries.

Dr. Okwudire was the recipient of the International Symposium on Flexible Automation Young Investigator Award, the Society of Manufacturing Engineers Outstanding Young Manufacturing Engineer Award, the Society of Automotive Engineers (SAE) International Ralph Teetor Educational Award, the National Science Foundation CAREER Award, and the 2016 American Society of Mechanical Engineers (ASME) Dynamic Systems and Controls Division's Best Conference Paper in Mechatronics Award.